

## Article

# Enhanced Photocatalytic Degradation of Rhodamine-B under Led Light Using CuZnAl Hydrotalcite Synthesized by Co-Precipitation Technique

Van Nhung Vu <sup>1,\*</sup>, Thi Ha Thanh Pham <sup>1</sup>, Maiboun Chanthavong <sup>1</sup>, Tra Huong Do <sup>1</sup>, Thi Hien Lan Nguyen <sup>1</sup>, Quoc Dung Nguyen <sup>1</sup>  and Thi Kim Ngan Tran <sup>2,\*</sup> 

- <sup>1</sup> Faculty of Chemistry, Thai Nguyen University of Education, No 20 Luong Ngoc Quyen Street, Thai Nguyen City 24000, Vietnam; thanhpth@tnue.edu.vn (T.H.T.P.); maiboun.chtv@gmail.com (M.C.); huongdt.chem@tnue.edu.vn (T.H.D.); lanth.chem@tnue.edu.vn (T.H.L.N.); dungnq@tnue.edu.vn (Q.D.N.)
- <sup>2</sup> Institute of Applied Technology and Sustainable Development, Nguyen Tat Thanh University, Ho Chi Minh City 700000, Vietnam
- \* Correspondence: nhuongvv@tnue.edu.vn (V.N.V.); ngantk@ntt.edu.vn (T.K.N.T.)

**Abstract:** The co-precipitation method was employed to synthesize a set of ZnAl hydrotalcite materials modified by Cu<sup>2+</sup>. The synthesized materials have a similar lamellar structure to that of hydrotalcite. The distance between layers is in the range of 7.73–8.56 Å. The network parameters a and c ranged from 3.058 to 3.074 Å and from 23.01 to 24.44, respectively. According to the IUPAC classification, the composites possess a mesoporous structure which belongs to class IV, type H 3. Particularly, the absorption edge shifts strongly to the visible light region when increasing the molar ratio of Cu<sup>2+</sup> in the samples from 0 to 3.5. The photocatalytic activity of the synthetic materials was evaluated through the degradation efficiency of rhodamine-B (Rh-B) in the water and colorants in textile wastewater. The present study was the first to synthesize a material sample that contains a molar ratio of Cu<sup>2+</sup> in the range of 2.5–3.5 and has high catalytic activities. They were able to degrade Rh-B at a high concentration (100 ppm) with a conversion rate of approximately 90% after 240 min of irradiation using a 30 W LED light. The catalytic activity of the composites depends on the molar ratio of modified Cu<sup>2+</sup>, the value of environmental pH, the H<sub>2</sub>O<sub>2</sub> concentration and the irradiation time.

**Keywords:** photocatalyst; degradation; rhodamine-B; co-precipitation; characterization



**Citation:** Vu, V.N.; Pham, T.H.T.; Chanthavong, M.; Do, T.H.; Nguyen, T.H.L.; Nguyen, Q.D.; Tran, T.K.N. Enhanced Photocatalytic Degradation of Rhodamine-B under Led Light Using CuZnAl Hydrotalcite Synthesized by Co-Precipitation Technique. *Inorganics* **2022**, *10*, 89. <https://doi.org/10.3390/inorganics10070089>

Academic Editor: Roberto Nisticò

Received: 5 May 2022

Accepted: 16 June 2022

Published: 23 June 2022

**Publisher's Note:** MDPI stays neutral with regard to jurisdictional claims in published maps and institutional affiliations.



**Copyright:** © 2022 by the authors. Licensee MDPI, Basel, Switzerland. This article is an open access article distributed under the terms and conditions of the Creative Commons Attribution (CC BY) license (<https://creativecommons.org/licenses/by/4.0/>).

## 1. Introduction

ZnAl hydrotalcite materials have been of significant interest to researchers and scientists. The precursors used to synthesize these materials are also highly diverse, ranging from nitrate, chloride and sulfate salts with molar ratios of Zn<sup>2+</sup>/Al<sup>3+</sup> of 2:1; 3:1 and 4:1, respectively [1–5]. The XRD analysis results show that the Zn<sup>2+</sup>/Al<sup>3+</sup> molar ratios of approximately 2:1 and 1.5:1 were the most suitable for the structure of LDHs [1] and CuZnAl material [2]. The ZnAl materials were used as the modification substrate by various agents (e.g., Cu, Ti and Eu), as well as organic composites (e.g., EDTA and EDDS) [6,7]. Therefore, promising results of catalytic and adsorbent materials were obtained in environmental treatments.

Hydrotalcite materials MgAlCO<sub>3</sub> and ZnAlCO<sub>3</sub> modified by transition metals (for example, Cu<sup>2+</sup>, Co<sup>2+</sup>, Fe<sup>3+</sup>, Cr<sup>3+</sup>, and Ni<sup>2+</sup>) have been successfully synthesized, mainly by co-precipitation, yielding metal-supported catalysts, immobilized systems and forms of oxide film and nanooxides obtained by the calcination of hydrotalcite materials at a controlled temperature [7–9]. The obtained research results showed that the isomorphous substitution of transition metal ions in a brucite-like lattice leads to the appearance of oxidation–reduction centers in the sheets which may act as active sites for the catalytic oxidation reaction [8]. The synthesized hydrotalcite materials have a unique layered structure, high thermal stability, tunable components, acidic–basic properties and structure memory effects [9].

Hydrotalcite materials modified with  $\text{Cu}^{2+}$  ions have been successfully synthesized, characterized and applied as adsorbents, photocatalysts and catalysts in the various fields. For instance, MgCuAl hydrotalcites have been successfully synthesized according to the molar ratios of  $\text{Cu}^{2+}$  of 0; 0.07; 0.14; 0.21; 0.28; and 0.35 (total molars of  $\text{Cu}^{2+}$  and  $\text{Mg}^{2+}$  to  $\text{Al}^{3+}$  of 0.7:0.3) for the purpose of oxidizing styrene into styrene oxide and benzaldehyde [8]; whereas CuZnAl hydrotalcites were used for the adsorption of  $\text{Cu}^{2+}$  ions in electroplating wastewater [2].

However, the study of the systematic influence of the molar ratios of the  $\text{Cu}^{2+}$  ion on the ZnAlCO<sub>3</sub> hydrotalcite structure and the use of CuZnAlCO<sub>3</sub> materials as photocatalysts for the photocatalytic degradation of rhodamine-B at high concentrations using light 30 W LED visible light ( $\lambda > 400$  nm,  $\lambda_{\text{max}} = 464$  nm) has not been published. In the present study, we synthesized the ZnAlCO<sub>3</sub> substrate according to the molar ratio  $\text{Zn}^{2+}/\text{Al}^{3+} = 7:3$ , followed by modification with the  $\text{Cu}^{2+}$  ion with the molar ratios  $\text{Cu}^{2+}$  of 0; 0.5; 1.0; 1.5; 2.0; 2.5; 3.0; and 3.5 using the co-precipitation method. The characterization analysis of the synthesized material was performed using XRD, EDX, SEM, TEM, BET, and UV-Vis DRS. The catalytic activity of the hydrotalcites was then evaluated by the degradation reaction of Rh-B using the 30 W LED light. This article will provide the results of the structural characterization of CuZnAlCO<sub>3</sub> materials, evaluate the photocatalytic activity of the synthesized materials for the rhodamine-B degradation reaction, select the optimal conditions for the degradation process of rhodamine-B under visible light, and evaluate the pigments decomposing performance in sedge textile dyeing wastewater.

## 2. Results

### 2.1. Structural Properties of Hydrotalcites

#### 2.1.1. XRD

The results of the XRD patterns shown in Figure 1 reveal that all the material samples with typical peaks such as the crystal structures of hydrotalcite at diffraction angles of 11.6°, 23.4°, 34.8° and 60.5° corresponded to the lattice planes of (003), (006), (009) and (110), respectively [9,10]. Therefore, the H and CuH-n materials preserved the hydrotalcite structure. However, the peak height of the characteristic peaks of hydrotalcite structure at the planes of (003), (009) and (110) decreased with the increasing proportion of  $\text{Cu}^{2+}$  in the material [2,7]. Based on the distance values (*d*) between the layers of the hydrotalcites at the plane of (003) and (110), the *a* and *c* parameters were obtained, where the *a* parameter represents the cation–cation distance in the brucite layer and  $a = 2 \cdot d_{110}$ . The thickness of the brucite layer was characterized by parameter *c* and the inner layer spacing and was calculated according to the formula  $c = 3d_{003}$  [3,11,12]. The calculation of parameters *a* and *c* shown in Table 1 revealed that they fluctuated in the range from 3.058 to 3.074 Å and from 23.18 to 24.15 Å, respectively. These *a* and *c* parameters are typical for hydrotalcites with the presence of  $\text{CO}_3^{2-}$  anions in the interlayers [1,5,13]. In addition, the characteristic diffraction peak for the CuO crystal at diffraction angle  $2\theta = 35.5^\circ$  [9,14,15] appeared quite weakly in some samples with  $\text{Cu}^{2+}$  molar ratios from 1.5 to 3.5. This result was consistent with the composites' color in Table 1, indicating that the  $\text{Cu}^{2+}$  ion was well dispersed in the brucite lattice structure of the hydrotalcite which is caused by the isomorphic substitution of  $\text{Cu}^{2+}$  with  $\text{Zn}^{2+}$  in the Brucite network. This could be explained by the fact that the  $\text{Cu}^{2+}$  and  $\text{Zn}^{2+}$  ions had a quite close ionic radius (0.73 and 0.74 Å, respectively) [1,9,11]. Moreover, the appearance of CuO particles in the material structure also contributes to promote the catalytic activity of materials [15,16].

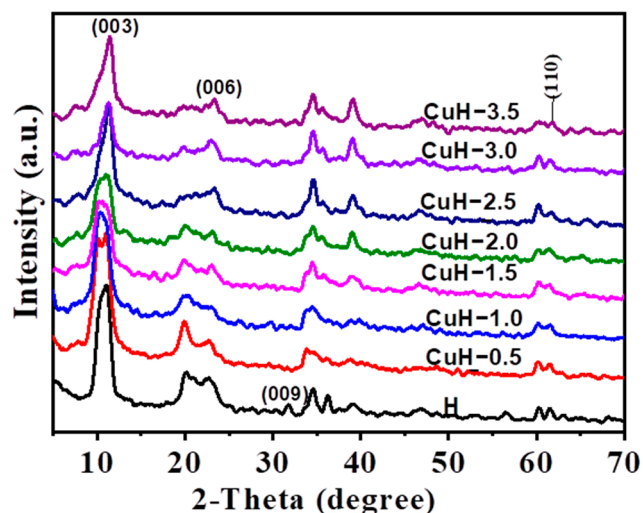


Figure 1. XRD pattern of the H and CuH-0.5–CuH-3.5 material samples.

Table 1. Analysis results percentage of elements O, Al, Cu, Zn in the H, CuH-3.0 hydrotalcites.

Samples	% O Atom	% Al Atom	% Cu Atom	% Zn Atom
H	72.19	8.94	0	18.87
CuH-3.0	79.04	8.78	5.32	6.86

Thus, the H and CuH-*n* materials synthesized with the molar ratio of  $\text{Cu}^{2+} = 0\text{--}3.5$  retained a similar lamellar structure to that of the hydrotalcite and the layered structure was slightly degraded when increasing the  $\text{Cu}^{2+}$  molar ratio. Especially, the production cost of hydrotalcites was significantly reduced using the pure chemicals from Xilong Scientific (Shantou, Guangdong, China), which helps reduce the cost of environmental treatment.

#### 2.1.2. SEM and TEM Images of the Materials

The SEM images of the H and CuH-3.0 hydrotalcites showed a lamellar structure (Figure 2a,b). The sample H contained hydrotalcite sheets with various sizes from small (30–50 nm) to large (>100 nm). In contrast, the CuH-3.0 material sample has more uniform slabs, and the plate size fluctuates in the range from 50 to 100 nm. However, the average grain size of the H and CuH-*n* materials ranges from 15 to 33 nm (Table 1). This result is also similar to Wu et al. (2020) [7]. Overall, the H and CuH-*n* materials were successfully synthesized with a hydrotalcite-like layered structure using the co-precipitation method and affordable chemicals with high purity.

The TEM images of the two materials samples H and CuH-3.0 clearly showed the lamellar structure of the hydrotalcites (Figure 2c,d). The plates of the H material had a lighter color than those of the CuH-3.0 material, while the colors of the CuH-3.0 sheets were bold and uniformly distributed. This result proves that  $\text{Cu}^{2+}$  ions are well-dispersed in the brucite network of hydrotalcite and benefit from the XRD characteristics of the composite samples.

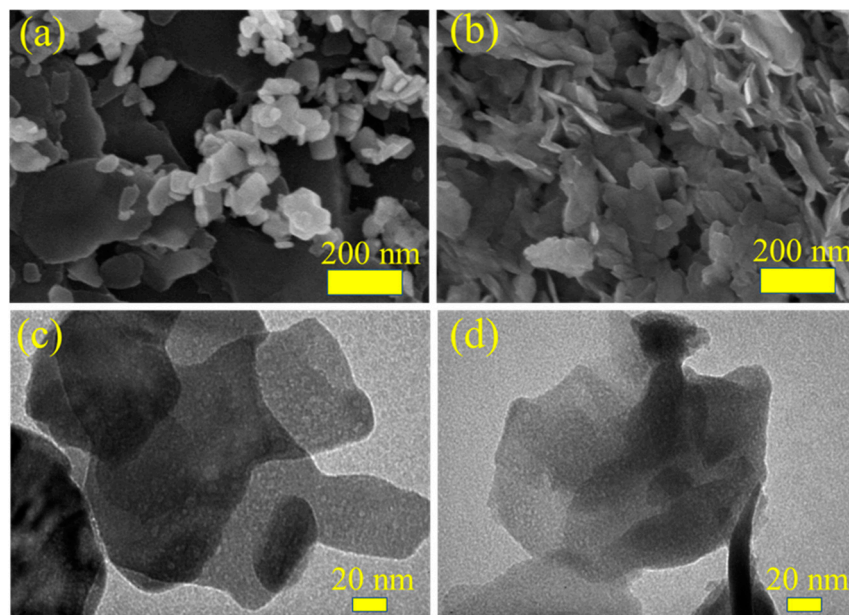


**Figure 2.** SEM images of the H (a) and CuH-3.0 hydrotalcites (b), TEM images of H (c) and CuH-3.0 samples (d).

### 2.1.3. Analysis Results of the Composition of Elements in the H and CuH-3.0 Hydrotalcites

The results of EDX spectral analysis of the H and CuH-3.0 hydrotalcites showed that there were the three elements O, Zn and Al presented in sample H and all four elements O, Al, Cu and Zn presented in the material sample CuH-3.0 (Figure 3). The percentage of atomic elements O, Al, Cu and Zn in the two samples of H and CuH-3.0 was shown in Table 1. The ratio of Zn and Al atoms in H was closed to a 2:1 ratio. It was possible to attach the H material with the composition  $Zn_4Al_2CO_3(OH)_{12} \cdot 3H_2O$ . The actual molar ratio of  $Cu^{2+}$  and  $Zn^{2+}$  ions in the CuH-3.0 sample is 5.32:6.86, which is quite similar to the theoretically calculated ratio of  $Cu^{2+}$  and  $Zn^{2+}$  to synthesize material.

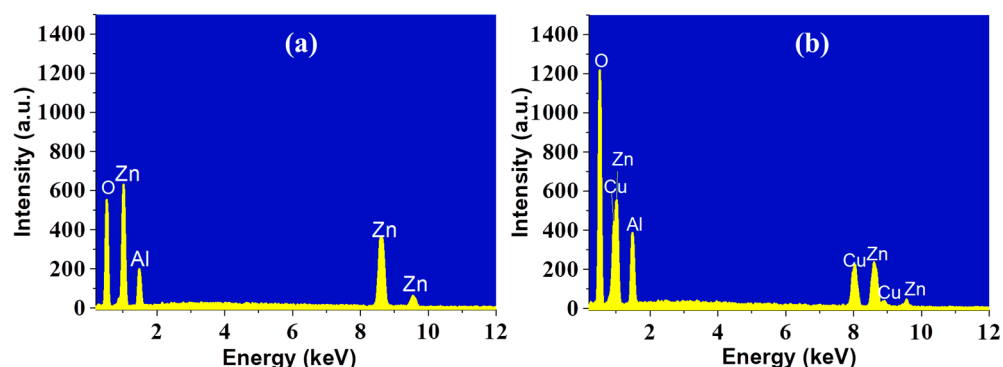


**Figure 3.** EDX spectrum of the H (a) and CuH-3.0 hydrotalcites (b).

### 2.1.4. The $N_2$ Adsorption/Desorption Isotherms (BET) of Hydrotalcites

The analysis results of  $N_2$  adsorption/desorption isotherms (BET) in Figure 4 showed that the two hydrotalcites H and CuH-1.0 had the  $N_2$  adsorption/desorption curves belonging to type IV and type H3, respectively, according to the IUPAC classification [2,11,17]. However, the two hydrotalcites CuH-2.0 and CuH-3.0 both had the  $N_2$  adsorption/desorption curves belonging to type IV and type H4 characterized by the mesoporous materials. The hysteresis of the adsorption isotherms and the desorption curves of the four hydrotalcites gradually increased with the increase in the molar ratio of  $Cu^{2+}$  in the sample. In general, when increasing the molar ratio of  $Cu^{2+}$  in the sample from 0 to 3.0, the specific surface area increased while the pore diameter reduced from 37.59 nm to 24.51 nm (Table 2).

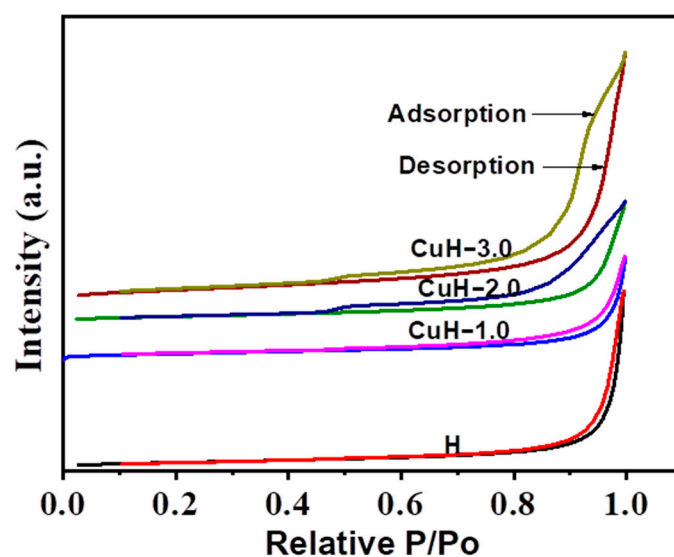


**Figure 4.** The  $N_2$  adsorption and desorption isotherms of four hydrotalcites: H, CuH-1.0, CuH-2.0 and CuH-3.0.

**Table 2.** Specific surface area (BET), pore diameter and pore volume of four hydrotalcites.

Sample	Surface Area BET (m <sup>2</sup> /g)	Porous Diameter (nm)	Porous Volume (cm <sup>3</sup> /g)
H	16.1	37.6	0.15
CuH-1.0	15.7	21.1	0.08
CuH-2.0	17.5	22.9	0.10
CuH-3.0	33.9	24.5	0.21

#### 2.1.5. UV-Vis DRS Spectra of Material Samples

The photocatalytic activity of the hydrotalcites can be predicted based on the UV-Vis DRS spectrum (Figure 5a). The H sample displayed two absorption peaks in the range of 220–350 nm in the UV light region. The light absorption in this range was attributed to the charge transfer from  $O^{2-}$  to metal cations ( $Al^{3+}$  and  $Zn^{2+}$ ) [13]. The UV-Vis spectral shape of the CuH-n materials was completely different from that of the H sample. The first absorption band was extended to a higher wavelength region (approximately 260 nm) which was explained by the charge transfer from  $O^{2-}$  to  $Cu^{2+}$  ions. In particular, there was a strong shift in the second absorption region to the visible light spectrum that could be explained by the charge displacement d-d in the octahedral medium of  $Cu^{2+}$  ions. Therefore, the absorption edge of the material also shifted strongly to the visible light region when increasing the ratio of  $Cu^{2+}$  in the material samples from 0.5 to 3.5.

Figure 5b illustrated the conversion to the bandgap energy of the hydrotalcites according to the equation of the Kubelka–Munk model fitted with indirect transition [18–20]. The bandgap energy  $E_g$  of the H and CuH samples decreased from 3.02 eV (H) to 2.3 eV (CuH-3.5). This result could indicate that the samples modified by  $Cu^{2+}$  possess good photocatalytic activity under visible light.

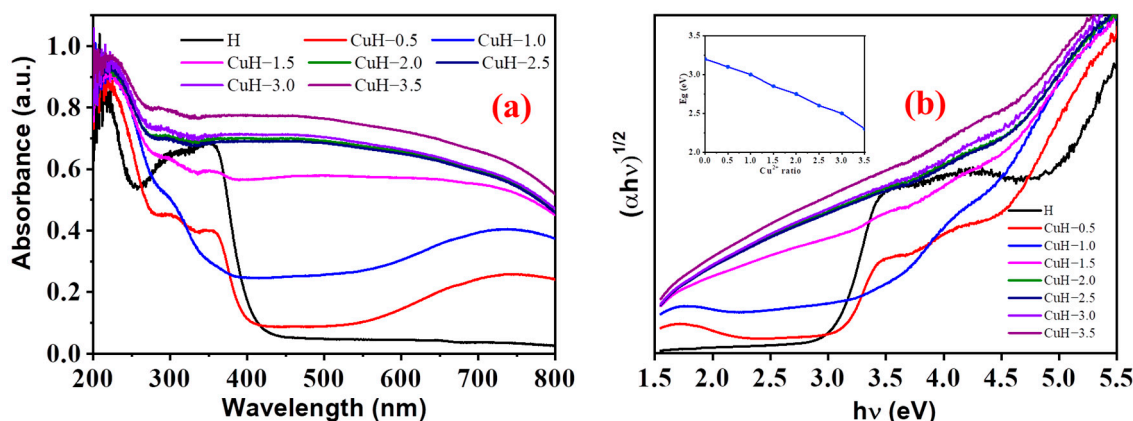


Figure 5. UV-Vis DRS spectrum (a) and band gap energy of composite samples (b).

## 2.2. Research on the Ability to Degrade Rh-B on Hydrotalcite Samples

### 2.2.1. Effect of the Dosage Cu<sup>2+</sup> ion in the Sample on the Catalytic Activity of the Material

The results of the 30 ppm Rh-B degradation activity of the hydrotalcites are shown in Figure 6. After 30 min of stirring in the dark to reach adsorption equilibrium, the 30 ppm Rh-B adsorption efficiency of all tested samples was equal to less than 10%. During irradiation under the 30 W LED light, the Rh-B degradation efficiency increased in accordance with the irradiation time. The 30 ppm Rh-B degradation sharply increased only after the first 30 min of illumination under the 30 W LED light and slowed down during the subsequent irradiation periods. After 30 min of irradiation, the Rh-B conversion reached 90–93% on the three samples of CuH-2.5, CuH-3.0 and CuH-3.5 materials.

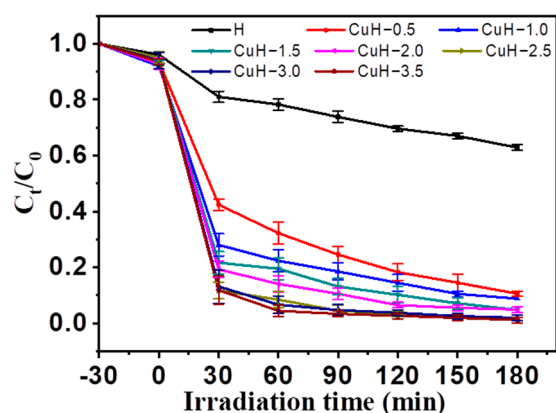
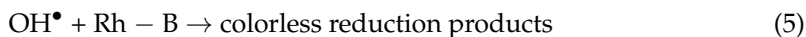
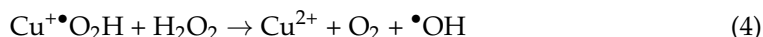


Figure 6. The 30 ppm Rh-B decolorization performance over irradiation time on hydrotalcites.

In contrast, the sample H exhibited the lowest ability to degrade Rh-B under the same tested conditions. The Rh-B conversion by this material was only 33% after 180 min of irradiation. The photocatalytic activity of CuH-n materials could be explained by the fact that the bandgap energy ( $E_g$ ) decreased when increasing the dosage of Cu<sup>2+</sup> in the sample. Furthermore, the 6500 K LED had three absorption peaks in the wavelength range from 446 to 477 nm and the strongest intensity was shown at the maximum wavelength of 464 nm [21], which was suitable for the light absorption region of CuH material samples to form photogenerated e<sup>-</sup> and h<sup>+</sup> pairs. In addition, Cu<sup>2+</sup> ions reacted with H<sub>2</sub>O<sub>2</sub> to generate the active intermediate radicals Cu<sup>+</sup>•O<sub>2</sub>H. Then, these active intermediate radicals continued to react with H<sub>2</sub>O<sub>2</sub> to produce Cu<sup>2+</sup>, O<sub>2</sub>, H<sub>2</sub>O and •OH radicals. Afterwards, •OH radicals targeted the chromogenic groups to degrade the Rh-B [20,22,23]:





Compared with the previous publications, all the H and CuH-n materials only insignificantly adsorbed Rh-B [19,24]. The first reason for this is that Rh-B, as a cationic dye, was unable to exchange anions with  $\text{CO}_3^{2-}$  ions in the interlayer. The second reason is the repulsion caused by metal ions in the plates for Rh-B molecules [11,25,26]. The activity of CuH materials mainly depends on the role of  $\text{Cu}^{2+}$  ions in the brucite network structure. The  $\text{Cu}^{2+}$  ions (1) reduced the activation energy of the materials; (2) enhanced the ability to absorb light in the visible light region; and (3) create catalytic centers that generate optical  $\bullet\text{OH}$  radicals. The role of  $\text{Cu}^{2+}$  ions in the hydrotalcites also reduced the recombination rate of  $e^- - h^+$  pairs, leading to an increasing rate of Rh-B degradation of these modified materials.

### 2.2.2. Effect of Rh-B Concentration on the Catalytic Activity of the Materials

The CuH-3.0 hydrotalcite sample was used to survey the Rh-B degradation ability in the selected concentration of Rh-B (Figure 7). The Rh-B ability degradation on the CuH-3.0 material sample gradually decreased with an increasing Rh-B concentration in the range of 30–100 ppm. The rate of Rh-B degradation rapidly increased after the first 30 min of irradiation at the concentrations of 30, 40 and 50 ppm of Rh-B. This rate slowly increased during the next 210 min. When the Rh-B concentration was 75 and 100 ppm, the Rh-B degradation efficiency gradually increased by 90% over approximately 240 min of the irradiation. Thus, it can be seen that the CuH-3.0 material was capable of degrading Rh-B at a high concentration of 100 ppm. It was proven that the H material modified by  $\text{Cu}^{2+}$  ions had obtained a new material with excellent photocatalytic activity towards the Rh-B degradation under the investigation conditions. This finding is the first to show that the synthesized hydrotalcites can degrade the Rh-B at high concentrations using only the 30 W LED light, resulting in lower disposal costs as compared to the 400 W halogen and the 500 W Xenon lights [18,24].

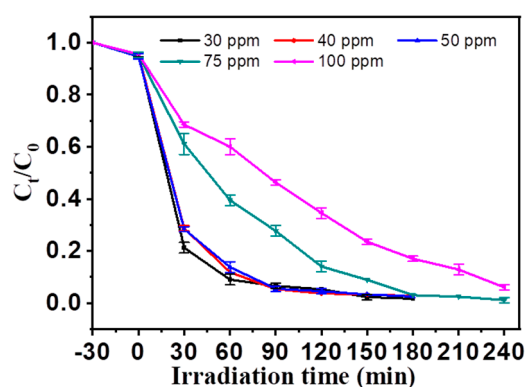


**Figure 7.** The comparison of the Rh-B degradation ability on the CuH-3.0 sample with the Rh-B concentrations are 30, 40, 50, 75 and 100 ppm.

### 2.2.3. Effect of $\text{H}_2\text{O}_2$ Concentration on the Catalytic Activity of the CuH-3.0 Material

As shown in Figure 8a, the catalytic activity of (1) the CuH-3.0 sample; (2) the combination of CuH-3.0 material sample and  $\text{H}_2\text{O}_2$  30%; and (3) the blank confirmed the role of oxidizing precursor to the Rh-B degradation of the material. The Rh-B degradation efficiency at the concentration of 100 ppm increased more slowly after 240 min of the irradiation in two cases—the blank and CuH-3.0. In contrast, the Rh-B degradation efficiency

rapidly increased when both the CuH-3.0 material and H<sub>2</sub>O<sub>2</sub> were combined, indicating that the catalytic activity of CuH-n material samples can be improved by combining with a low level of H<sub>2</sub>O<sub>2</sub>. Equations (1)–(4) explained the catalytic activity of CuH-n in the presence of H<sub>2</sub>O<sub>2</sub> to form the •OH photogenic radicals involved in Rh-B degradation.

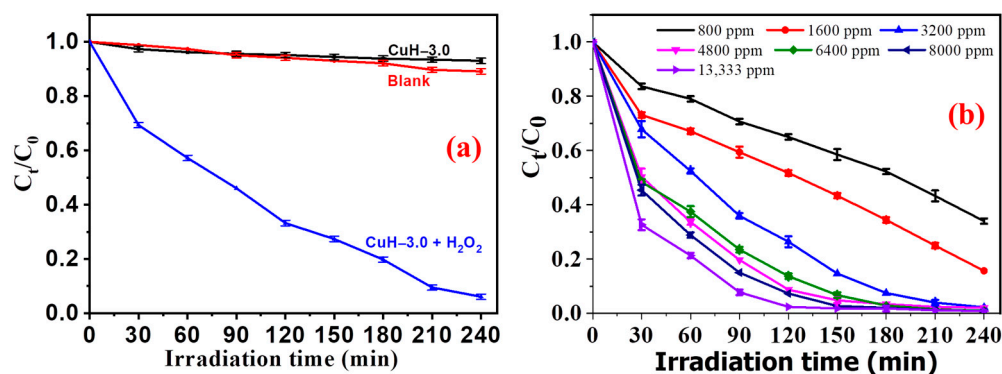


**Figure 8.** The comparison of the ability to degrade Rh-B at a concentration of 100 ppm in three cases (a) and the ability to degrade the Rh-B of CuH-3.0 at different concentrations of H<sub>2</sub>O<sub>2</sub> (b).

The influence of the H<sub>2</sub>O<sub>2</sub> concentration on the catalytic activity of CuH-3.0 hydrotalcite was shown in Figure 8b. The Rh-B degradation rate accelerated as the H<sub>2</sub>O<sub>2</sub> concentration increased from 800 to 13,333 mg/L. In particular, the Rh-B degradation efficiency at a concentration of 100 ppm could reach approximately 70% after only 30 min of irradiation in combination with the 13,333 mg/L H<sub>2</sub>O<sub>2</sub>.

The survey results can be explained by the fact that a high concentration of H<sub>2</sub>O<sub>2</sub> could promote the generation of more •OH photogenic radicals, thus increasing the rate of Rh-B degradation: H<sub>2</sub>O<sub>2</sub> → 2 •OH. However, excessively high H<sub>2</sub>O<sub>2</sub> concentration would hinder the Rh-B degradation rate and complicate the removal procedure. The reduced catalytic activity of the material at high H<sub>2</sub>O<sub>2</sub> concentrations is explained by the fact that the generated •OH radicals react with H<sub>2</sub>O<sub>2</sub> to produce •OOH radicals and O<sub>2</sub> molecules that are much weaker oxidizing agents than •OH radicals [27].



#### 2.2.4. Effect of Medium pH on the Catalytic Activity of the Material

The medium pH values clearly influenced the catalytic activity of the CuH-3.0 material sample (Figure 9). The catalytic activity of the material decreased when changing the medium pH values of the 100 ppm Rh-B solution from the initial pH of 5.06 to the acidic region and the basic region. In a strongly acidic environment (pH = 2.0), the catalytic activity of the material decreased strongly. This result was due to the destruction of the structure of the material at a strong acidic pH media and the decreasing number of Cu<sup>2+</sup> catalyst sites caused by leaching to the solution [28–30]. The catalytic activity of the material also decreased when increasing the medium pH value from 5.06 to the neutral, basic and strong base regions (pH = 10.0–12.0). This result was explained by the fact that the increasing solution viscosity at a high pH value reduced the diffusivity of Rh-B to the material surface and the light absorption by the material. In addition, the structure of the material could be destroyed by dissolving Zn(OH)<sub>2</sub> and Al(OH)<sub>3</sub> at a high pH value. Therefore, the optimal pH range for degrading the Rh-B of the material was the slightly acidic pH range of 5.06–6.0.

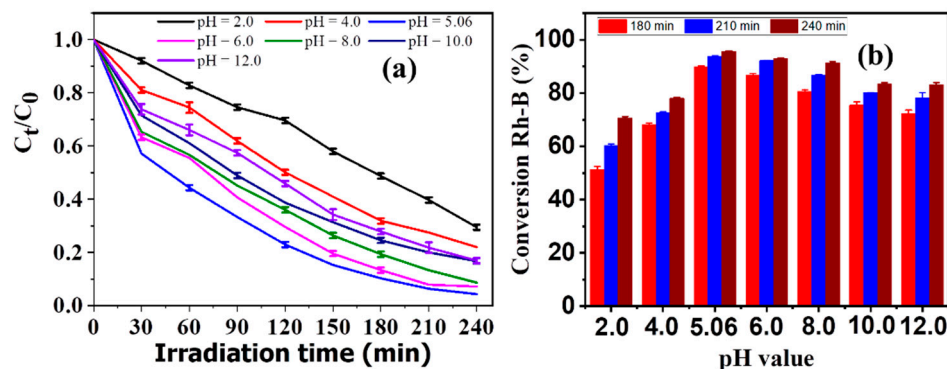


**Figure 9.** The comparison in the degradation ability of Rh-B at 100 ppm concentration of CuH-3.0 sample at different environmental pH values (a) and conversion Rh-B of 100 ppm at 180, 210, 240 min (b).

With the obtained survey results, it can be seen that the photocatalytic activity of CuH-n materials was significantly enhanced, depending on the main factors: the ratio molar of  $\text{Cu}^{2+}$  ion in the sample, lighting time, medium pH value and  $\text{H}_2\text{O}_2$  concentration. It is possible to diagram the Rh-B decomposition reaction by the CuH-n photocatalyst in Figure 10 below.

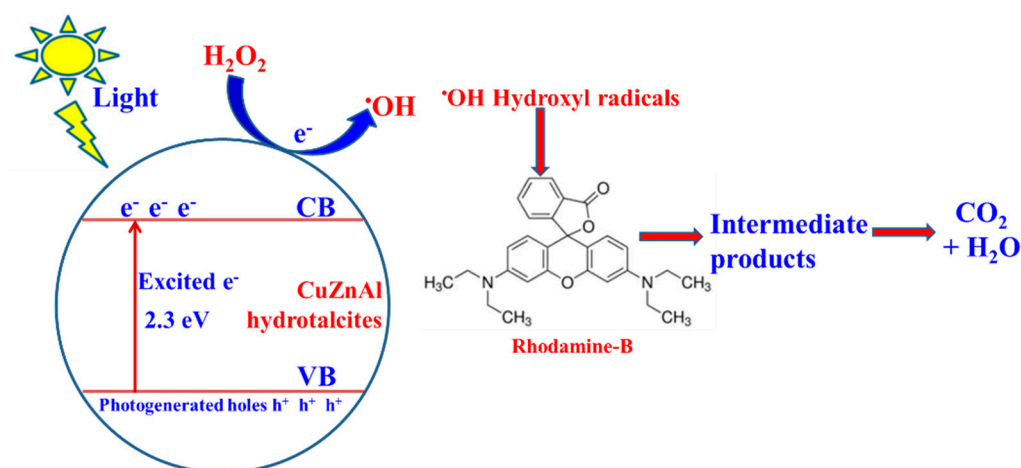


**Figure 10.** Schematic diagram of Rh-B photocatalytic degradation on CuH-n hydroxalcite.

### 2.3. Applications to Textile Wastewater Treatment

Due to the complex composition of wastewater and the addition of color stabilizers, 5.0 mL of 30%  $\text{H}_2\text{O}_2$  solution was used in this experiment. The survey results showed that the intensity of the absorption peaks of the pigments at 500–553 nm gradually decreased with the irradiation time at pH 3.52 (Figure 11b). Such a decrease in the intensity became significant at pH 6.0 (Figure 11c). This result is in closed agreement with the investigation of the optimal conditions of the material for Rh-B. However, the degradation efficiency of pigments in wastewater was only approximately 88% after 360 min of lighting at pH 6.0 (Figure 11a). The obtained results concluded that the CuH-3.0 material can completely decompose the pigments in the textile wastewater composition, thus introducing the potential application of CuH-n material samples in textile wastewater treatment.

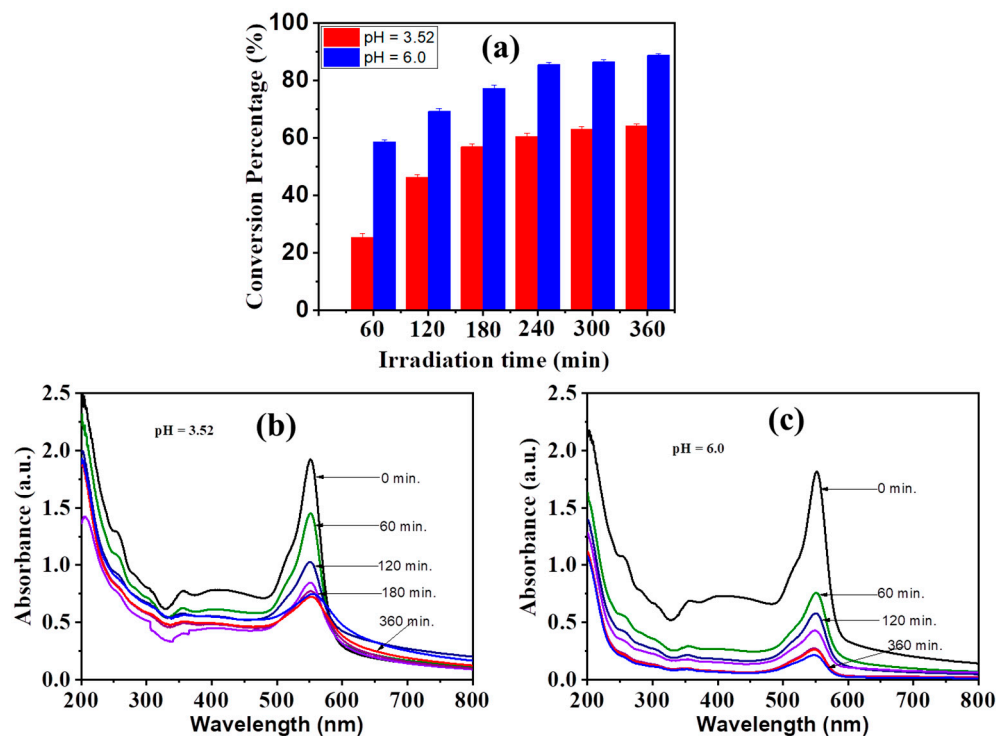


**Figure 11.** Conversion of dyes in the textile dyeing wastewater composition at pH 3.52 and 6.0 (a), the UV-Vis spectrum of dyes in the survey progress after 360 min of the irradiation by 30 W LED light at pH = 3.52 (b), pH = 6.0 (c).

### 3. Materials and Methods

#### 3.1. Materials

Zinc nitrate ( $\text{Zn}(\text{NO}_3)_2 \cdot 6\text{H}_2\text{O}$ ), aluminum nitrate ( $\text{Al}(\text{NO}_3)_3 \cdot 9\text{H}_2\text{O}$ ) and Rh-B were purchased from Xilong Scientific, China. Copper nitrate ( $\text{Cu}(\text{NO}_3)_2 \cdot 3\text{H}_2\text{O}$ ), sodium carbonate ( $\text{Na}_2\text{CO}_3$ ), sodium hydroxide ( $\text{NaOH}$ ), Rh-B and 30% hydrogen peroxide solution ( $\text{H}_2\text{O}_2$ ) were purchased from Merck, Darmstadt, Germany. The chemicals have a purity of more than 99%.

#### 3.2. Synthesis of the Materials

The hydrotalcite material  $\text{ZnAl-CO}_3$  (H) and hydrotalcites modified by  $\text{Cu}^{2+}$  ions (denoted as CuH-n) were synthesized following the co-precipitation method described by Wu et al. (2020) with minor modifications [3,7,8,31]. Briefly,  $\text{Al}(\text{NO}_3)_3 \cdot 9\text{H}_2\text{O}$ ,  $\text{Zn}(\text{NO}_3)_2 \cdot 6\text{H}_2\text{O}$  and  $\text{Cu}(\text{NO}_3)_2 \cdot 3\text{H}_2\text{O}$  were simultaneously dissolved with 150 mL of deionized water in the 250 mL triangle vessel. The precursor salts were collected and adjusted to obtain the molar ratio  $(\text{Cu}^{2+} + \text{Zn}^{2+})/\text{Al}^{3+} = 7:3$  (Table 3). The reaction vessel was placed on a heated magnetic stirrer to obtain a homogeneous solution. Then, 25 mL of 0.6 M  $\text{Na}_2\text{CO}_3$  solution was added dropwise to the reaction flask and stirred for 60 min at room temperature. The resulting mixture was transferred to a 500 mL beaker and the pH of the mixture was adjusted to 9.5 by 2M  $\text{NaOH}$  solution, allowing gel formation. The gel was then stirred on a magnetic stirrer for 60 min and aged in a Teflon flask at 100 °C for 24 h. After aging, the synthesized gel was filtrated and washed with hot deionized water (70 °C) several times until pH = 7.0. The solids were dried at 80 °C for 24 h to obtain the samples of hydrotalcite  $\text{ZnAlCO}_3$  (H) and hydrotalcites modified by  $\text{Cu}^{2+}$  ions (denoted as CuH-n where n is the molar ratio of  $\text{Cu}^{2+}$  in the sample). Finally, the samples were ground with an agate mortar and pestle and used for the subsequent experiments.

**Table 3.** The characterization of sample of ZnAl and Cu<sup>2+</sup> modified hydrotalcites ( $n_{\text{Zn}} + n_{\text{Cu}} = 0.07$ ,  $n_{\text{Al}} = 0.03$ ,  $n_{\text{CO}_3} = 0.015$  (mol)]).

No.	Name	Molar Ratio Cu:Zn:Al:CO <sub>3</sub>	d <sub>003</sub> (Å)	d <sub>006</sub> (Å)	d <sub>110</sub> (Å)	Average Grain Size in Scherrer (nm)	Lattice Parameter (Å)		Color
							A	c	
1	H	0:7.0:3.0:1.5	8.025	3.929	1.534	33.28	3.068	24.075	White
2	CuH-0.5	0.5:6.5:3.0:1.5	8.027	3.913	1.537	18.64	3.074	24.081	Light blue
3	CuH-1.0	1.0:6.0:3.0:1.5	8.559	3.866	1.536	20.31	3.072	25.677	Light blue
4	CuH-1.5	1.5:5.5:3.0:1.5	8.051	3.854	1.535	17.96	3.07	24.153	Black blue
5	CuH-2.0	2.0:5.0:3.0:1.5	7.963	3.841	1.537	15.09	3.074	23.889	Black
6	CuH-2.5	2.5:4.5:3.0:1.5	7.806	3.812	1.536	21.20	3.072	23.418	Black
7	CuH-3.0	3.0:4.0:3.0:1.5	7.824	3.868	1.535	16.09	3.07	23.472	Black
8	CuH-3.5	3.5:3.5:3.0:1.5	7.726	3.808	1.529	19.02	3.058	23.178	Black

### 3.3. Structures and Catalytic Properties of Materials

The crystalline phase composition of the synthesized samples was characterized by X-ray diffraction (XRD) on the D8-ADVANCE 5005-Brucker instrument (Bruker AXS, Karlsruhe, Germany). The light shifting edge band gap energy was determined by the UV-Vis DRS spectra on a HITACHI U-4100 spectrometer (Tokyo, Japan). The specific surface area was determined by the N<sub>2</sub> adsorption–desorption isotherm (BET) on a MicroActive for TriStar II Plus Version 2.03 instrument (Micromeritics, Norcross, GA, USA). The SEM and TEM images of the material were taken by using the Hitachi S-4800 instrument, Jeol 3010 (Tokyo, Japan). The elemental composition was determined by EDX spectroscopy using the HORIBA instrument (MODEL 7593-H) (Kyoto, Japan).

### 3.4. Evaluation of the Catalytic Efficiency of Synthesized Materials through the rhodamine-B Decomposition Reaction

The Rh-B degradation efficiency of the synthesized material was evaluated through the following survey. A 30 W LED lamp which has a 6500 K color temperature (Philips, Amsterdam, The Netherlands) was used as the visible light source. The reaction mixture of 250 mL Rh-B solution and 0.2 g of the material was stirred in the dark for 30 min until the adsorption equilibrium was achieved. Then, 1.2 mL of 30% H<sub>2</sub>O<sub>2</sub> was added to the reaction mixture and the sampling of Rh-B concentration was carried out every 30 min and centrifuged and the molecular absorbance was measured at the wavelength of 553 nm. The materials with good activity were selected to investigate the influence of Rh-B concentrations, H<sub>2</sub>O<sub>2</sub> concentration and medium pH value and its application to treat sedge mat textile wastewater. The survey experiments were conducted 3 times. The results were then calculated to obtain the average values as well as the standard error values and used to evaluate the photocatalytic activity of the investigated materials.

### 3.5. Determination of Rh-B Concentration in Water

The standard curve for determining the Rh-B concentration in water was followed by equation  $y = 0.1674x + 0.0069$  ( $R^2 = 0.9994$ ). The standard curve for determining the Rh-B concentration is shown in Figure 12 below.

After the degradation progress, the concentration of Rh-B in the water was determined. For every 30 min of irradiation, a small amount (5–7 mL) of Rh-B sample was extracted from the reaction mixture and centrifuged to remove the sample material. The samples were diluted before measuring the absorbance of Rh-B at 553 nm on a Shimadzu UV–Vis 1700 instrument. The concentration of Rh-B remaining in the solution was calculated according to the calibration curve from Figure 12.

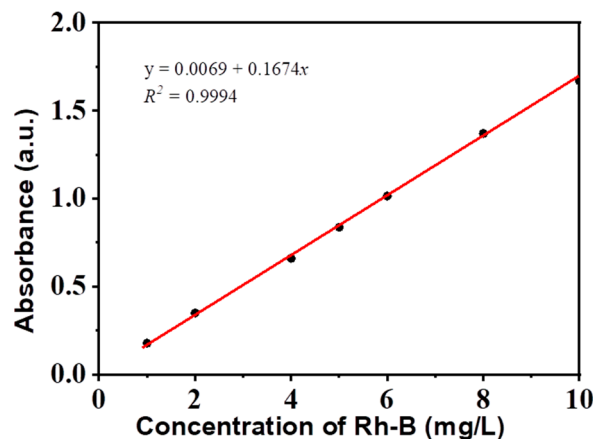


Figure 12. Standard curve for determination of Rh-B concentration in the water.

### 3.6. Research on the Ability to Treat Textile Wastewater

Dark red-colored sewage sludge mats containing a high concentration of pigments was collected from the wastewater tank of households located in Dong Bang village, Quynh Phu district, Thai Binh province, Vietnam. Prior to the experiment, the initial wastewater sample was diluted ten times with distilled water. Then, the diluted wastewater sample (250 mL) was investigated for the ability to degrade the colorants in wastewater according to the following parameters: the initial medium pH value of 3.52, and the adjusted pH value of 6.0 and 0.2 g of CuH-3.0 material sample. All reaction mixtures were contained in a 500 mL beaker and sealed with a black glossy bag. Afterwards, the reaction mixture was stirred in the dark for 30 min to reach adsorption equilibrium. The 5.0 mL of 30% H<sub>2</sub>O<sub>2</sub> solution was added to the reaction mixture. The reaction mixtures were irradiated under a 30 W LED light at room temperature. The samples were collected to determine the pigments' degradability of the composite after a period of every 60 min. After the sample was centrifuged to remove a small amount of catalyst, the wastewater was diluted 10 times for UV-Vis spectrum scanning on a UV 1700 SHIMADZU machine (Kyoto, Japan). The color degradation efficiency was calculated based on the absorbance of the pigments at wavelengths of 550–553 nm. The survey experiments were conducted 3 times. The results are then calculated to obtain average values, standard error values and used to evaluate the photodegradation ability for colorants in textile dyeing wastewater.

$$H\% = \frac{Abs_0 - Abs_t}{Abs_0} \times 100 (\%) \quad (9)$$

Here,  $Abs_0$  and  $Abs_t$  is the absorbance of colorant at the initial time and sampling time, respectively.

## 4. Conclusions

The H and CuH-n-synthesized hydrotalcites possess a similar layered structure as hydrotalcite, despite a decrease in structure when increasing the molar ratio of Cu<sup>2+</sup> ion in the brucite layers from 0 to 3.5. The results of XRD pattern characterization showed the presence of weak peaks of the crystalline phase of CuO in the samples with a molar ratio of Cu<sup>2+</sup> from 1.5 to 3.5. The catalytic activity of H samples modified by Cu<sup>2+</sup> ions increased significantly. The survey results indicated that the catalytic activity of the materials depends on various factors, such as the molar ratio of Cu<sup>2+</sup> ions in the sample, the irradiation time, the concentration of rhodamine-B, the concentration of H<sub>2</sub>O<sub>2</sub> and the medium pH value. The hydrotalcite samples with the molar ratio of Cu<sup>2+</sup> ions in the range of 2.5–3.5 exhibit the highest photocatalytic activity for Rh-B degradation. The presence of a small amount of H<sub>2</sub>O<sub>2</sub> significantly increased the ability to degrade Rh-B at a 100 ppm concentration on the CuH-3.0 sample. In addition, the medium pH value in the slightly acidic range (5.06–6.0) provided the most favorable environment for Rh-B degradation. In addition, the

CuH-3.0 material sample can completely degrade the pigments in textile wastewater. The conversion efficiency of colorants in wastewater can reach up to 88%. Simultaneously, the color intensity of the mixture significantly decreased, and the solution became pale after 360 min of illumination. The results of the structural characterization and photocatalytic activity of the synthesized samples confirmed that the materials modified by the Cu<sup>2+</sup> molar ratio of 2.5–3.5 are considered an excellent photocatalyst for the degradation of the high Rh-B concentration and the textile wastewater treatment.

**Author Contributions:** Conceptualization, M.C. and T.H.L.N.; methodology, M.C. and Q.D.N.; software, T.H.L.N. and Q.D.N.; formal analysis, T.K.N.T. and T.H.T.P.; data curation, V.N.V.; writing—original draft preparation, T.H.T.P., V.N.V. and T.H.D.; writing—review and editing, T.H.D. and T.K.N.T. All authors have read and agreed to the published version of the manuscript.

**Funding:** The authors would like to sincerely thank the financial resources from the project CS.2021.23 of the University of Education, Thai Nguyen University.

**Institutional Review Board Statement:** Not applicable.

**Informed Consent Statement:** Not applicable.

**Data Availability Statement:** All the data are available within the manuscript.

**Conflicts of Interest:** The authors declare no conflict of interest.

## References

1. Cursino, A.C.T.; da Silva Lisboa, F.; dos Santos Pyrrho, A.; de Sousa, V.P.; Wypych, F. Layered Double Hydroxides Intercalated with Anionic Surfactants/Benzophenone as Potential Materials for Sunscreens. *J. Colloid Interface Sci.* **2013**, *397*, 88–95. [[CrossRef](#)] [[PubMed](#)]
2. Bai, D.; Wang, X.; Huo, D.; Ying, Q.; Wang, N.; Xia, B. Coprecipitation Preparation of Cu/Zn/Al-Hydrotalcite-like Compound for Copper Removal from Electroplating Wastewater. *J. Chem.* **2019**, *2019*, 5347920. [[CrossRef](#)]
3. Mahjoubi, F.Z.; Khalidi, A.; Abdennouri, M.; Barka, N. Zn–Al Layered Double Hydroxides Intercalated with Carbonate, Nitrate, Chloride and Sulphate Ions: Synthesis, Characterisation and Dye Removal Properties. *J. Taibah Univ. Sci.* **2017**, *11*, 90–100. [[CrossRef](#)]
4. Amor, F.; Diouri, A.; Ellouzi, I.; Ouanji, F.; Kacimi, M. High Efficient Photocatalytic Activity of Zn-Al-Ti Layered Double Hydroxides Nanocomposite. In *MATEC Web of Conferences*; EDP Sciences: Les Ulis, France, 2018; Volume 149, p. 1087.
5. Chen, Y.; Li, F.; Yu, G.; Yang, X. Fluorescence of Zn–Al–Eu Ternary Layered Hydroxide Response to Phenylalanine. *Spectrochim. Acta Part A Mol. Biomol. Spectrosc.* **2012**, *86*, 625–630.
6. Zhang, S.; Kano, N.; Imaizumi, H. Synthesis and Characterization of LDHs (Layered Double Hydroxides) Intercalated with EDTA (Ethylenediaminetetracetic Acid) or EDDS (N, N'-1, 2-Ethanediybis-1-Aspartic Acid). *J. Environ. Sci. Eng. A* **2016**, *5*, 549–558. [[CrossRef](#)]
7. Wu, L.; Peng, B.; Li, Q.; Wang, Q.; Yan, X.; Li, K.; Lin, Q. Effects of Cu<sup>2+</sup> Incorporation on ZnAl-Layered Double Hydroxide. *New J. Chem.* **2020**, *44*, 5293–5302.
8. Thao, N.T.; Huyen, L.T.K. Catalytic Oxidation of Styrene over Cu-Doped Hydrotalcites. *Chem. Eng. J.* **2015**, *279*, 840–850. [[CrossRef](#)]
9. Jia, M.; Zhang, Y.; Bao, Y.; Wang, J.; Xu, A. Recyclable CuMgAl Hydrotalcite for Oxidative Esterification of Aldehydes with Alkylbenzenes. *Green Chem. Lett. Rev.* **2018**, *11*, 230–236. [[CrossRef](#)]
10. Xia, S.; Zhang, L.; Pan, G.; Qian, P.; Ni, Z. Photocatalytic Degradation of Methylene Blue with a Nanocomposite System: Synthesis, Photocatalysis and Degradation Pathways. *Phys. Chem. Chem. Phys.* **2015**, *17*, 5345–5351. [[CrossRef](#)]
11. Parida, K.; Mohapatra, L.; Baliarsingh, N. Effect of Co<sup>2+</sup> Substitution in the Framework of Carbonate Intercalated Cu/Cr LDH on Structural, Electronic, Optical, and Photocatalytic Properties. *J. Phys. Chem. C* **2012**, *116*, 22417–22424. [[CrossRef](#)]
12. Ramos-Ramirez, E.; Gutiérrez-Ortega, N.; Tzompantzi, F.; Gomez, C.M.; del Angel, G.; Herrera-Pérez, G.; Serafín-Muñoz, A.H.; Tzompantzi-Flores, C. Activated Hydrotalcites Obtained by Coprecipitation as Photocatalysts for the Degradation of 2, 4, 6-Trichlorophenol. *Adv. Mater. Sci. Eng.* **2018**, *2018*, 8267631. [[CrossRef](#)]
13. Jabłońska, M.; Chmielarz, L.; Węgrzyn, A.; Góra-Marek, K.; Piwowarska, Z.; Witkowski, S.; Bidzińska, E.; Kuśtrowski, P.; Wach, A.; Majda, D. Hydrotalcite Derived (Cu, Mn)–Mg–Al Metal Oxide Systems Doped with Palladium as Catalysts for Low-Temperature Methanol Incineration. *Appl. Clay Sci.* **2015**, *114*, 273–282. [[CrossRef](#)]
14. Zeng, Y.; Zhang, T.; Xu, Y.; Ye, T.; Wang, R.; Yang, Z.; Jia, Z.; Ju, S. Cu/Mg/Al Hydrotalcite-like Hydroxide Catalysts for o-Phenylphenol Synthesis. *Appl. Clay Sci.* **2016**, *126*, 207–214. [[CrossRef](#)]
15. Zhang, H.; Tang, C.; Lv, Y.; Sun, C.; Gao, F.; Dong, L.; Chen, Y. Synthesis, Characterization, and Catalytic Performance of Copper-Containing SBA-15 in the Phenol Hydroxylation. *J. Colloid Interface Sci.* **2012**, *380*, 16–24. [[CrossRef](#)]

16. Lee, S.S.; Bai, H.; Liu, Z.; Sun, D.D. Novel-Structured Electrospun TiO<sub>2</sub>/CuO Composite Nanofibers for High Efficient Photocatalytic Cogeneration of Clean Water and Energy from Dye Wastewater. *Water Res.* **2013**, *47*, 4059–4073. [[CrossRef](#)]
17. Argote-Fuentes, S.; Feria-Reyes, R.; Ramos-Ramírez, E.; Gutiérrez-Ortega, N.; Cruz-Jiménez, G. Photoelectrocatalytic Degradation of Congo Red Dye with Activated Hydrotalcites and Copper Anode. *Catalysts* **2021**, *11*, 211. [[CrossRef](#)]
18. Chuaicham, C.; Sekar, K.; Balakumar, V.; Zhang, L.; Trakulmututa, J.; Smith, S.M.; Sasaki, K. Fabrication of Hydrotalcite-like Copper Hydroxyl Salts as a Photocatalyst and Adsorbent for Hexavalent Chromium Removal. *Minerals* **2022**, *12*, 182. [[CrossRef](#)]
19. Zhu, Y.; Zhu, R.; Zhu, G.; Wang, M.; Chen, Y.; Zhu, J.; Xi, Y.; He, H. Plasmonic Ag Coated Zn/Ti-LDH with Excellent Photocatalytic Activity. *Appl. Surf. Sci.* **2018**, *433*, 458–467. [[CrossRef](#)]
20. Nguyen, L.T.T.; Nguyen, H.T.T.; Le, T.H.; Nguyen, L.T.H.; Nguyen, H.Q.; Pham, T.T.H.; Bui, N.D.; Tran, N.T.K.; Nguyen, D.T.C.; Lam, T.V. Van. Enhanced Photocatalytic Activity of Spherical Nd<sup>3+</sup> Substituted ZnFe<sub>2</sub>O<sub>4</sub> Nanoparticles. *Materials* **2021**, *14*, 2054. [[CrossRef](#)]
21. Chaopu, Y.; Wenqing, F.; Jiancheng, T.; Fan, Y.; Yanfeng, L.; Chun, L. Change of Blue Light Hazard and Circadian Effect of LED Backlight Displayer with Color Temperature and Age. *Opt. Express* **2018**, *26*, 27021–27032. [[CrossRef](#)]
22. Wang, L.; Kong, A.; Chen, B.; Ding, H.; Shan, Y.; He, M. Direct Synthesis, Characterization of Cu-SBA-15 and Its High Catalytic Activity in Hydroxylation of Phenol by H<sub>2</sub>O<sub>2</sub>. *J. Mol. Catal. A Chem.* **2005**, *230*, 143–150. [[CrossRef](#)]
23. Nguyen, L.T.T.; Vo, D.-V.N.; Nguyen, L.T.H.; Duong, A.T.T.; Nguyen, H.Q.; Chu, N.M.; Nguyen, D.T.C.; Van Tran, T. Synthesis, Characterization, and Application of ZnFe<sub>2</sub>O<sub>4</sub>@ZnO Nanoparticles for Photocatalytic Degradation of Rhodamine B under Visible-Light Illumination. *Environ. Technol. Innov.* **2022**, *25*, 102130. [[CrossRef](#)]
24. Chen, G.; Qian, S.; Tu, X.; Wei, X.; Zou, J.; Leng, L.; Luo, S. Enhancement Photocatalytic Degradation of Rhodamine B on NanoPt Intercalated Zn–Ti Layered Double Hydroxides. *Appl. Surf. Sci.* **2014**, *293*, 345–351. [[CrossRef](#)]
25. Arofah, N.; Ahmad, E.F. Zn-Al Hydrotalcite As Adsorbent on Metal Waste (Cu<sup>2+</sup>): Case Study of Liquid Waste in Integrated Laboratory Center UIN Syarif Hidayatullah. In Proceedings of the International Conference on Science and Technology (ICOSAT 2017)-Promoting Sustainable Agriculture, Food Security, Energy, and Environment Through Science and Technology for Development, Ancol, Indonesia, 10 August 2017; Atlantis Press: Paris, France, 2017; pp. 143–147.
26. Djaballah, R.; Bentouami, A.; Benhamou, A.; Boury, B.; Elandaloussi, E.H. The Use of Zn-Ti Layered Double Hydroxide Interlayer Spacing Property for Low-Loading Drug and Low-Dose Therapy. Synthesis, Characterization and Release Kinetics Study. *J. Alloys Compd.* **2018**, *739*, 559–567. [[CrossRef](#)]
27. Akpan, U.G.; Hameed, B.H. Parameters Affecting the Photocatalytic Degradation of Dyes Using TiO<sub>2</sub>-Based Photocatalysts: A Review. *J. Hazard. Mater.* **2009**, *170*, 520–529. [[CrossRef](#)]
28. Zaghouane-Boudiaf, H.; Boutahala, M.; Arab, L. Removal of Methyl Orange from Aqueous Solution by Uncalcined and Calcined MgNiAl Layered Double Hydroxides (LDHs). *Chem. Eng. J.* **2012**, *187*, 142–149. [[CrossRef](#)]
29. Berner, S.; Araya, P.; Govan, J.; Palza, H. Cu/Al and Cu/Cr Based Layered Double Hydroxide Nanoparticles as Adsorption Materials for Water Treatment. *J. Ind. Eng. Chem.* **2018**, *59*, 134–140. [[CrossRef](#)]
30. Mandal, S.; Mayadevi, S. Adsorption of Fluoride Ions by Zn–Al Layered Double Hydroxides. *Appl. Clay Sci.* **2008**, *40*, 54–62. [[CrossRef](#)]
31. Maru, M.S.; Patel, P.; Khan, N.H.; Shukla, R.S. Copper Hydrotalcite (Cu-HT) as an Efficient Catalyst for the Hydrogenation of CO<sub>2</sub> to Formic Acid. *Curr. Catal.* **2020**, *9*, 59–71. [[CrossRef](#)]